

PAPER

## A constitutive model and its numerical implementation for reversible behavior of shape memory hydrogels

To cite this article: Yunqiang Hu *et al* 2022 *Smart Mater. Struct.* **31** 095032

View the [article online](#) for updates and enhancements.

### You may also like

- [Quadruple-shape hydrogels](#)  
Maria Balk, Marc Behl and Andreas Lendlein

- [Statistical Study of Small-scale Magnetic Holes in the Upstream Regime of the Martian Bow Shock](#)  
G. Q. Wang, M. Volwerk, A. M. Du et al.

- [Profitability, income inequality, and subjective well-being of mariculture households in China](#)  
Jing Wu, Hongbo Yang and Wu Yang

# A constitutive model and its numerical implementation for reversible behavior of shape memory hydrogels

Yunqiang Hu<sup>1</sup>, Fei Jia<sup>1,\*</sup>, Zijian Fu<sup>2</sup>, Yanju Liu<sup>1</sup>  and Jinsong Leng<sup>2,\*</sup> 

<sup>1</sup> Department of Astronautical Science and Mechanics, Harbin Institute of Technology ( HIT ),  
PO Box 301, No. 92 West Dazhi Street, Harbin 150001, People's Republic of China

<sup>2</sup> Center for Composite Materials and Structures, Science Park of Harbin Institute of Technology ( HIT ),  
PO Box 3011, No. 2 YiKuang Street, Harbin 150080, People's Republic of China

E-mail: [feijia@hit.edu.cn](mailto:feijia@hit.edu.cn) and [lengjs@hit.edu.cn](mailto:lengjs@hit.edu.cn)

Received 17 May 2022, revised 23 June 2022

Accepted for publication 18 July 2022

Published 2 August 2022



## Abstract

Shape memory hydrogels (SMHs) are kinds of smart materials with great importance in many fields, such as drug release and soft robotics. In order to design the structures base on SMHs, it is necessary to reveal the mechanism of the shape memory effect and establish the constitutive model of SMHs. However, the existing constitutive models can not describe some of important mechanical behavior of SMHs, such as reversible shape memory effects. In this paper, a three-dimensional finite deformation constitutive model is developed for SMHs with reversible shape memory effects caused by the conformation transition of N-isopropylacrylamide (PNIPAM). In order to well capture its reversible shape memory effect, the polymer network for PNIPAM is decomposed into two parts, coil PNIPAM and globule PNIPAM, with different reference configurations. Then this model is implemented into a user material subroutine (UMAT) and is used for simulating the equilibrium swelling, isothermal uniaxial tension, reversible shape memory behavior and multiple shape memory cycles of SMHs. Our model is validated by comparing the simulation results with experiments. The deformation of a more complex 3D structure and a bilayer structure containing SMHs are also numerically studied which demonstrates great potential of our model in exploring the application of SMHs.

Keywords: shape memory hydrogels, constitutive model, numerical implementation, reversible behavior

(Some figures may appear in colour only in the online journal)

## 1. Introduction

Shape memory hydrogels (SMHs) can fix temporary shapes and recover to their initial shapes under specific external stimuli (temperature, PH, salt, etc), on account of their shape memory effect [1–3]. Compared to shape memory polymers (SMPs), SMHs can exhibit large deformations exceeding 2600% while highly stretchable SMPs cannot undergo or

recover from strains of over 1000% [4]. Besides, the interaction between polymer network and the solutions of SMHs enables the heating-triggered and cooling-triggered shape recovery, and reversible shape memory behavior [5–7]. Due to these excellent properties, SMHs have promising applications in many fields, i.e., drug release and soft robotics [8–10].

Conventional thermal response N-isopropylacrylamide (PNIPAM) hydrogels could undergo reversible volume changes as shown in figure 1(a) during heating and cooling [11]. However, the volume change is entirely influenced by the water content and is not called as shape memory effect.

\* Authors to whom any correspondence should be addressed.

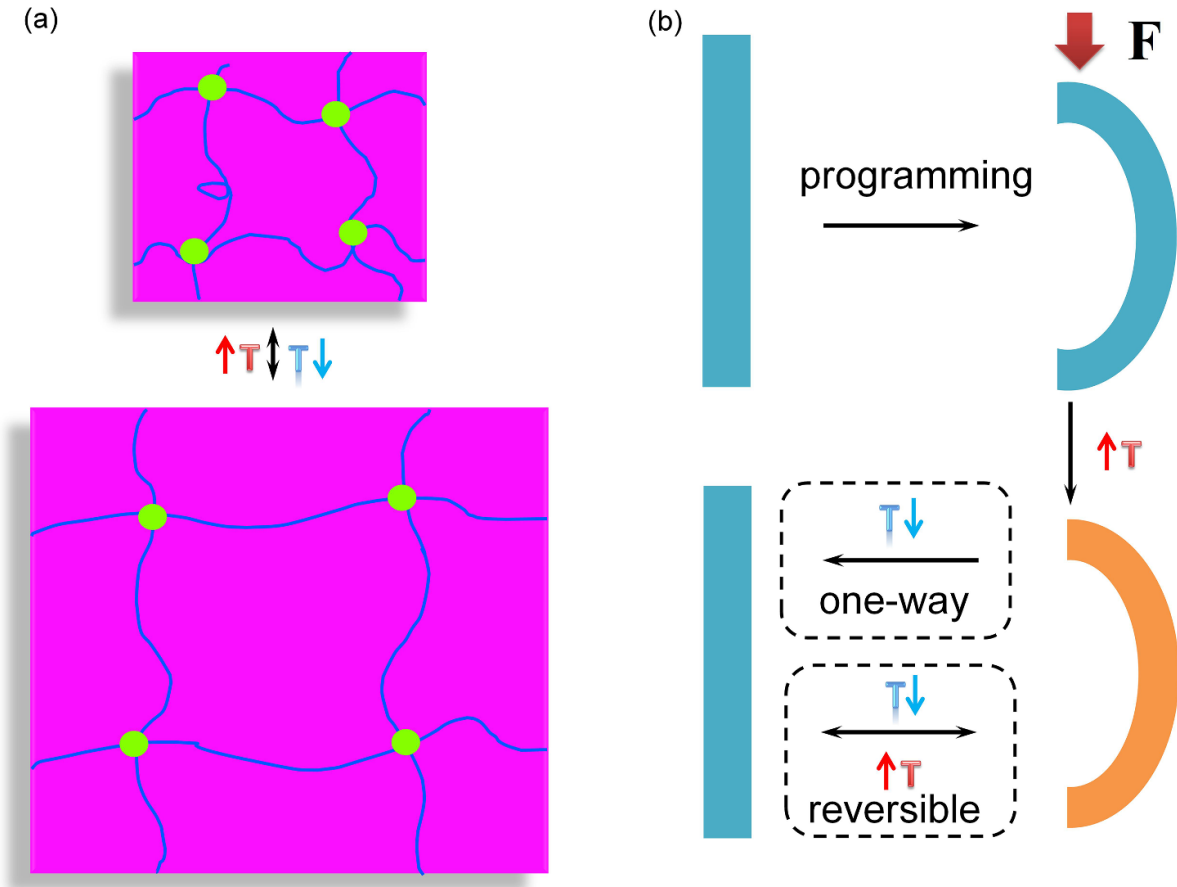


**Figure 1.** (a) The volume changes of conventional thermal response hydrogels. (b) Schematic of shape memory process of one-way and reversible SMHs.

Other than conventional hydrogels, SMHs have the merit of programmability, which means that the desired shape can be designed and recorded under external stimuli and loading. Shape memory effect of hydrogel was reported for the first time [5]. Subsequently, many works investigated the shape memory effect of hydrogels, from material synthesis to applications [9, 10, 12, 13]. However, most of them focus on one-way SMHs which limit their implication because one-way SMHs cannot return to temporary shape again after changing temperature (figure 1(b)). Recently, Liu *et al* [7] reported a kind of two-way SMH with cooling-triggered shape recovery based on transient structural anisotropy caused by conformation transition of PNIPAM chain which overcomes this shortcoming. The reversible shape memory process is described as follows (figure 1(b)): The SMH is predeformed from a swollen state to a deformed shape at low temperature. Then the deformed shape is kept during the temperature rising. This shape could be largely preserved to reach a temporary shape even after removing the external load. SMH can return to its initial shape (In fact, this shape is close to the initial shape but not exactly the initial shape, and for simplicity, we call it the initial shape.) after cooling and recovering to the temporary shape after reheating. Compared with heating-triggered shape recovery hydrogels, this kind of cooling-triggered shape

recovery hydrogels are more suitable for human body, as high temperature causes irreversible tissue damage, whereas proteins and cells can tolerate temperatures down to the freezing point of water [6].

Due to the importance of stimuli-response hydrogels, much effort has been dedicated to reveal its mechanical mechanisms and develop constitutive models [11, 14, 15]. Details of advances can be found in a recent review [16], but these models do not focus on the shape memory effect of hydrogels. Although the constitutive models of SMPs are well established [17–21], for SMHs these models are no longer suitable in most cases due to differences in the shape memory mechanisms. At the microscopic level, the shape memory behavior of SMHs can be achieved through two different strategies, dynamic covalent bonds and supramolecular interactions [22]. The former one is accomplished by stimuli-controllable decoupling and coupling of dynamic covalent linkages, while the latter one is through dynamic association and dissociation of non-covalent interactions, i.e. hydrogen bonds and hydrophobic interaction [22–24]. As a kind of important supramolecular hydrogels, PNIPAM based hydrogels have been extensively studied due to their temperature-sensitive conformational transition behavior, such as volume phase transition [11, 25], but less work is about shape memory effect.

Molecular mechanism of PNIPAM based SMHs is revealed as following (figure 2(a)): PNIPAM undergoes a conformational transition (coil to globule) [26, 27] where the temporary shape is fixed. Through cooling, the PNIPAM undergoes reversible conformational transition (globule to coil) and the SMH is able to return to its initial shape. This is essentially caused by the temperature sensitivity of the hydrophobic interaction.

Recently, a phenomenological constitutive model has been established for double network SMHs [28]. However, the existing models are still insufficient to describe reversible behavior of SMHs. In this work, combining micro-mechanisms and thermodynamic framework, we develop a constitutive model of SMHs with reversible shape memory effect by polymer network decomposition methods.

This paper is organized as follows. Section 2 proposes a constitutive model of reversible SMHs. We identify parameters of the constitutive model and implement this model into a user material subroutine (UMAT) in section 3. The simulation results of equilibrium swelling, isothermal temperature uniaxial stretching, reversible shape memory effect and multiple shape memory cycling process of SMHs are compared with experimental results in sections 4 and 5 is the conclusion.

## 2. Constitutive model

### 2.1. Overall description

We established a constitutive model of SMHs through polymer network decomposition method [29, 30]. According to the state of PNIPAM (coil or globule), the network of SMHs can be divided into two networks, network A and network B, with different reference configurations shown in figure 2(b). The reference configuration of network A is independent of the programming deformation while the reference configuration of network B is related to the programming deformation. The volume fraction of network A and network B correspond to the fraction of coil and globule PNIPAM chain, respectively. More details about network A and network B can be found in section 2.4.

### 2.2. Framework of constitutive model

In this model, deformation gradient  $\mathbf{F} = \partial\mathbf{x}/\partial\mathbf{X}$  is defined to measure the deformation.  $\mathbf{X}$  and  $\mathbf{x}$  denote the positions in initial and deformed configuration, respectively. We split the overall deformation gradient into swelling part  $\mathbf{F}_S$  and mechanical part  $\mathbf{F}_M$  by multiplicative decomposition [31, 32]

$$\mathbf{F} = \mathbf{F}_M \mathbf{F}_S, \quad (1)$$

where  $\mathbf{F}_S$  represents the deformation gradient of the SMH from the dry network state ( $\tilde{\Omega}$ ) to the stress-free swollen state ( $\Omega_0$ ) and  $\mathbf{F}_M$  represents the mechanical deformation after equilibrium swelling. We consider that if SMH is in swelling equilibrium state which means the stress equals zero although the polymer network has been deformed due to water molecules migration. Assuming that the swelling deformation is isotropic [33],  $\mathbf{F}_S$  can be further written as  $\mathbf{F}_S = \lambda_S \mathbf{I}$ ,  $I$

is the second-order identity tensor and  $\lambda_S$  is swelling stretch which characterizes the stretching of the network due to water molecules into the polymer network.

The relationship between deformation gradient of two networks and  $\mathbf{F}_M$  is

$$\begin{aligned} \mathbf{F}_M &= \mathbf{F}_A \\ \mathbf{F}_M &= \mathbf{F}_B \mathbf{H}, \end{aligned} \quad (2)$$

where  $\mathbf{F}_A$ ,  $\mathbf{F}_B$  are deformation gradient of A and B network, respectively.  $\mathbf{H}$  represents the deformation of reference configuration of network B, and its evolution equation is given in section 2.4. The total volume change of SMH is  $J = \det \mathbf{F} = J_M J_S$  and  $J_S = \lambda_S^3 = 1 + c\nu$ , where  $c$  is the number of moles of water molecules contained in the initial configuration and  $\nu$  is the volume of per mole of water molecules.

The relationship between the physical quantities in the constitutive model follows the law of thermodynamics. This thermodynamics framework can be derived as [34]

$$\psi + \eta \dot{T} - \mathbf{P} : \dot{\mathbf{F}} - \mu \dot{c} + \frac{1}{T} \mathbf{q} \cdot \nabla T + \mathbf{j} \cdot \nabla \mu \leq 0, \quad (3)$$

where  $\psi = \psi(\mathbf{C}_A, \mathbf{C}_B, c, T)$  is the Helmholtz free energy density function,  $\mathbf{P}$  is first Piola-Kirchhoff stress,  $\eta$  is the entropy,  $\mu$  is chemical potential and  $T$  is absolute temperature in Kelvin.

For the convenience of considering SMHs shape memory effects, the free energy density function is summed by the free energy due to swelling and that due to mechanical deformation of SMHs [35]. The former one includes two parts. First part is the free energy  $\psi_{\text{mix}}(c, T)$  caused by mixing the polymer network and water molecules. Another part is the free energy  $\psi_0$  from stretching the polymer network during initial free swelling process. We further divide the free energy due to mechanical deformation of SMHs into the free energy of deformation  $\psi_A$  and  $\psi_B$  of the A and B networks according to the constitutive model of SMHs. Therefore, the free energy of SMHs is written as

$$\psi = \psi_0 + \psi_{\text{mix}}(c, T) + f_C \psi_A(\mathbf{C}_A, T) + f_G \psi_B(\mathbf{C}_B, T), \quad (4)$$

where,  $f_C$  and  $f_G$  are the fraction of coil chain and globule chain, respectively. Since the total number of PNIPAM chains is constant, we have  $f_C + f_G = 1$ . The mixing free energy is given as [25, 36, 37]

$$\psi_{\text{mix}}(c, T) = RTc \left( \ln \left( \frac{\nu c}{1 + \nu c} \right) + \frac{\chi}{1 + \nu c} \right), \quad (5)$$

where  $\chi$  is called interaction parameter and  $R$  is the ideal gas constant. Many models can describe the mechanical deformation of SMHs. Considering the large deformation characteristics of polymer networks, utilizing the eight-chain model [38] based on the non-Gaussian statistical chains [39], the free energy due to mechanical deformation is given as

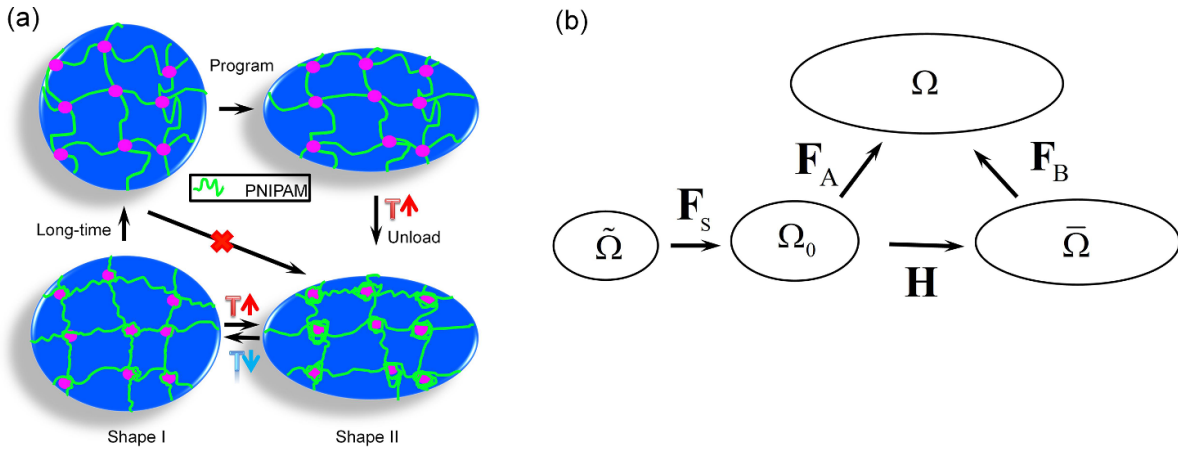


**Figure 2.** (a) Molecular mechanism of shape memory effect in SMHs. (b) An analogous decomposition scheme for deformation gradient.

$$\begin{aligned} & f_C \psi_A(\mathbf{C}_A, T) + f_G \psi_B(\mathbf{C}_B, T) \\ &= f_C \left[ N_A n_A k_b T \left( \frac{\bar{\lambda}_A \beta_A}{\sqrt{n_A}} + \ln \frac{\beta_A}{\sinh \beta_A} \right) + \frac{1}{2} K_A (\ln J_A)^2 \right] \\ &+ f_G \left[ N_B n_B k_b T \left( \frac{\bar{\lambda}_B \beta_B}{\sqrt{n_B}} + \ln \frac{\beta_B}{\sinh \beta_B} \right) + \frac{1}{2} K_B (\ln J_B)^2 \right], \end{aligned} \quad (6)$$

where  $N_A, N_B$  are the number of total polymer chains per unit volume,  $n_A, n_B$  are the number of Kuhn segments and  $k_b$  is the Boltzmann constant. For network A and B,  $\beta = \mathcal{L}^{-1}(\bar{\lambda}/\sqrt{n})$  and  $\mathcal{L}^{-1}(x)$  is the inverse Langevin function. The Langevin function is defined as  $\mathcal{L}(x) = \coth(x) - 1/x$ . Also for network A and B,  $\bar{\lambda} = \sqrt{I_1/3}$ , where  $I_1 = \text{tr}(\bar{\mathbf{B}})$  with  $J^{\frac{2}{3}} \bar{\mathbf{B}} = \mathbf{F} \mathbf{F}^T$  and  $J = \det(\mathbf{F})$ .

After a more complex derivation, the Cauchy stress and the chemical potential are obtained as (the detailed derivation is given in appendix)

$$\begin{aligned} \sigma &= f_C \left[ \frac{\mu_A \sqrt{n_A}}{3 J_A \bar{\lambda}_A} \mathcal{L}^{-1} \left( \frac{\bar{\lambda}_A}{\sqrt{n_A}} \right) \left( \bar{\mathbf{B}}_A - \frac{1}{3} \text{tr}(\bar{\mathbf{B}}_A) \mathbf{I} \right) \right. \\ &\quad \left. + \frac{1}{J_A} K_A \ln J_A \mathbf{I} \right] \\ &+ f_G \left[ \frac{\mu_B \sqrt{n_B}}{3 J_B \bar{\lambda}_B} \mathcal{L}^{-1} \left( \frac{\bar{\lambda}_B}{\sqrt{n_B}} \right) \left( \bar{\mathbf{B}}_B - \frac{1}{3} \text{tr}(\bar{\mathbf{B}}_B) \mathbf{I} \right) \right. \\ &\quad \left. + \frac{1}{J_B} K_B \ln J_B \mathbf{I} \right] \end{aligned} \quad (7)$$

and

$$\mu = RT(\ln(1 - \phi) + \phi + \chi\phi^2) - \frac{1}{3} J_M \sigma_{mm} \nu, \quad (8)$$

respectively.  $\phi = 1/(1 + \nu c)$  is volume fraction of polymer network.

### 2.3. Fraction of globule chain

As described in section 2.1, we divide the network of SMHs into two parts according to the conformational state of

the PNIPAM chain and  $f_G(T)$  is ascertained in present section. The conformation transition of PNIPAM is that the evolution of the structure of a single PNIPAM chain after the environment has been changed from a good solvent to a poor solvent and vice versa [40]. Many studies have shown that the conformational transition of PNIPAM chain is a temperature, time and current deformation dependent process [27, 40–42]. The governing equation of this transition process can be written as [26]

$$\xi^5 - \xi^3 - \frac{p}{\xi^3} - q = 0, \quad (9)$$

where,  $\xi = R(T)/R(T_\theta)$  is collapse ratio [43].  $T_\theta$  denotes the  $\theta$ -point temperature,  $R(T)$  denotes the radius of chain at current temperature and  $R(T_\theta)$  represents the radius of chain at  $T_\theta$ , while  $p$  and  $q$  are governing parameters. As shown in figure 3(a), when  $p > 0.02278$ ,  $\xi$  monotonically changes with  $q$ , while  $p < 0.02278$ ,  $\xi$  dose not monotonically change with  $q$ . This non-monotonic change means that the PNIPAM chain undergoes a first phase transition process which corresponds to volume phase transition at the macroscopic level.

In this work, since the water content did not change much during the experiment, we simplify the conformational transition of PNIPAM as a continuous process, and the fraction of globule chain  $f_G(T)$  is expressed as monotonic and continuous function  $f_G(T) = (1 - \gamma)f(T)$ .  $f(T)$  is the relationship between the fraction of globule chain and temperature when the end of chain is in free. The form of  $f(T)$  is assumed as

$$f(T) = \frac{1}{2} \left[ 1 + \tanh \left( \frac{T - T_\theta}{\Delta} \right) \right] (1 - \exp(-\Xi)), \quad (10)$$

where,  $T_\theta$  and  $\Delta$  are material parameters. Because the conformational transition of PNIPAM needs some time to reach equilibrium, a parameter  $\Xi$  is introduced and represents the ratio of experiment time to characteristic time of conformation transition. If  $\Xi \gg 1$ ,  $f_G$  equals to the equilibrium value when temperature changes. If  $\Xi$  is close to or less than 1,  $f_G$  does not equal to the equilibrium value when temperature changes.  $\gamma$  represents the stretch effect on conformation transition of chain. If  $\gamma$  is close 1, that is, the length of chain is close to

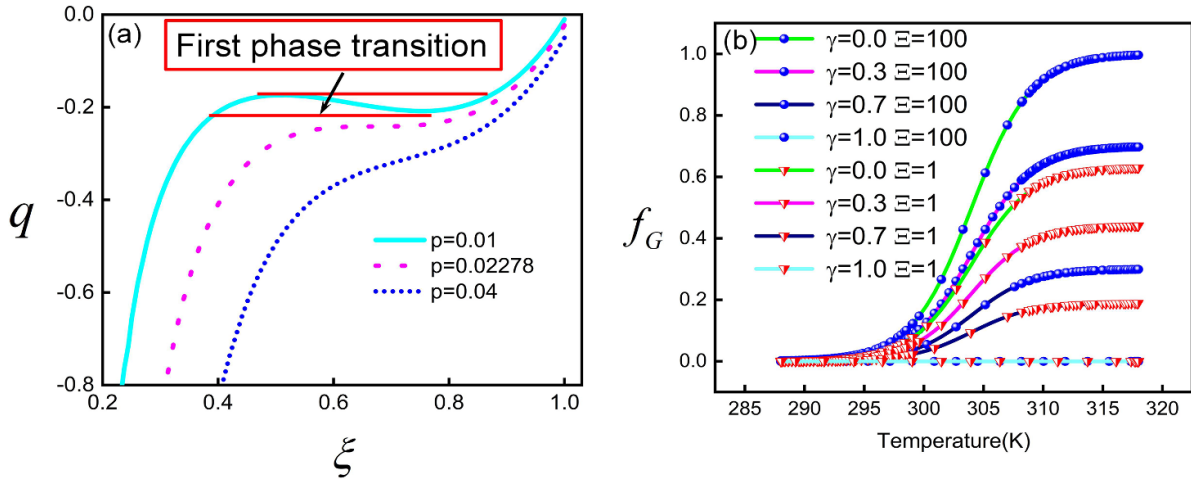


**Figure 3.** (a) Plot of the curves between  $\xi$  and the governing parameter  $q$ , according to equation (9). (b) Plot of the fraction of globule chain in equilibrium  $f_G$  as a function of temperature  $T$ , calculated by equation (11).

its contour length, the PNIPAM chain cannot transform into globule chain when temperature changes. Then the fraction of globule chain is written as

$$f_G(T) = \frac{1}{2} (1 - \gamma) \left[ 1 + \tanh \left( \frac{T - \Delta}{\Delta} \right) \right] (1 - \exp(-\Xi)). \quad (11)$$

For different  $\gamma$  and  $\Xi$ , the curves between  $f_G$  and temperature are shown in figure 3(b). It is clear that  $f_G$  decreases as  $\gamma$  increasing and  $\Xi$  decreasing. Considering that the network of SMH is cross-linked by numerous molecular chains and each of which may have different fraction of globule chain due to different deformation, to reduce the cost of the calculation,  $\gamma$  is assumed as a constant and the effect of  $\gamma$  on shape memory behavior of SMHs is discussed in section 4.5.

#### 2.4. Evolution equations

**2.4.1. Reference configuration of network B.** As mentioned in section 2.1, the reference configuration  $\mathbf{H}$  of network B is assumed to be changed with the current configuration of network A. It is necessary to establish the evolution equation of  $\mathbf{H}$ . We focus on the macroscopic phenomenal model to achieve shape memory effect of SMHs rather than the complex behaviors of molecular chains, so we assume that the newly transformed network B takes the current configuration as its reference configuration. Similar approaches are often used to develop constitutive models of SMPs [20, 44, 45]. The deformation gradient of the reference configuration of network B is assumed as

$$\mathbf{H}_{n+1} = \begin{cases} (\mathbf{F}_B)_n^{-1} \mathbf{F}_n & \Delta T > 0 \\ \bar{\mathbf{H}}_{n+1} & \Delta T \leq 0 \end{cases}, \quad (12)$$

where  $n$  and  $n+1$  indicate the present and previous increments, respectively.  $\bar{\mathbf{H}}(\varpi, \tau)$  represents the reference conformational deformation gradient associated with the reversible shape memory cycle.  $\varpi$  is the total immersion time

in low-temperature water after SMH shape memory programming.  $\tau$  is the time of the disappearance of shape memory effect when SMH is immersed in water with low temperature.

**2.4.2. Attenuation of the reference configuration.** Experiment finds SMH can transform repeatedly between the two intermediate configurations when temperature changes between high temperature and low temperature. The shape fixed ratio gradually decreases and finally disappears as the increasing of total duration time at low temperature [7]. Decreasing of shape fixed ratio means different mechanical behavior among each low-high temperature cycle. In the model, decreasing of shape fixed ratio can be considered through the decay reference configuration of network B from current configuration to initial configuration (same as that of network A). We propose the evolution equation of the reference configuration of network B as

$$\bar{\mathbf{H}} = \begin{cases} \mathbf{F}^* & \varpi = 0 \\ \mathbf{I} & \varpi = \tau \end{cases}, \quad (13)$$

where  $\mathbf{F}^*$  is the deformation gradient of the reference configuration of the part B network at the end of the SMH programming. The eigenvalues and eigenvectors  $\lambda_i, \mathbf{N}_i$  ( $i = 1, 2, 3$ ) of  $\bar{\mathbf{C}} = \bar{\mathbf{H}}^T \bar{\mathbf{H}}$  can be defined as

$$\lambda_i = (\lambda_i^* - 1)\Upsilon(\varpi, \tau) + 1 \quad (14)$$

and

$$\mathbf{N}_i = \mathbf{N}_i^*, \quad (15)$$

respectively, where  $\lambda_i^*, \mathbf{N}_i^*$  are the corresponding components of  $\mathbf{C}^* = \mathbf{F}^{*T} \mathbf{F}^*$ .

Considering that  $\det \bar{\mathbf{H}} = 1$ , the deformation gradient of the reference configuration is defined as

$$\bar{\mathbf{H}} = \sum_{i=1}^3 \sqrt{\lambda_i} \mathbf{N}_i \otimes \mathbf{N}_i. \quad (16)$$

For  $\Upsilon(\varpi, \tau)$ , a time boundary condition

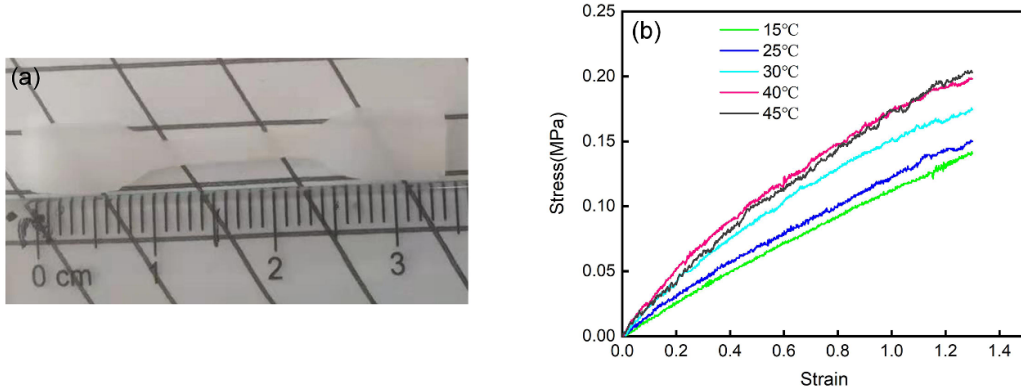


**Figure 4.** (a) Tensile specimen of the SMH. (b) Stress–strain curves of the SMH from isothermal uniaxial tension tests at different temperatures.

$$\Upsilon(\varpi, \tau) = \begin{cases} 1 & \varpi = 0 \\ 0 & \varpi \rightarrow \tau \end{cases} \quad (17)$$

must be satisfied to match equation (13) and here we assume as

$$\Upsilon(\varpi, \tau) = e^{A(1 + \frac{\tau}{\varpi - \tau})}, \quad (18)$$

where  $A$  is material parameter.

### 3. Parameter determination and FE implementation

#### 3.1. Parameter determination

The values of the material parameters are identified by water content tests and isothermal uniaxial tensile tests. Equilibrium water content tests at different temperatures and shape memory process of SMH have been studied [7], so we add isothermal uniaxial tensile experiments of SMH at different temperatures.

The materials were synthesized following the procedure published in [7]. The dimension of the dumbbell type tensile specimen is  $35\text{ mm} \times 5\text{ mm} \times 0.8\text{ mm}$  and the stretching velocity is  $20\text{ mm min}^{-1}$ . During shape memory cycling, the water content of SMH did not change much [7], so we tested the mechanical behavior of SMH at different temperatures in a non-equilibrium state. The SMH was immersed in water at  $15^\circ\text{C}$  for 6 h to reach swelling equilibrium. The SMH was placed at a specific temperature ( $15^\circ\text{C}$ ,  $25^\circ\text{C}$ ,  $30^\circ\text{C}$ ,  $40^\circ\text{C}$ ,  $45^\circ\text{C}$ ) for 3 min and then subjected to a tensile test. This process is very fast compared to the hydrogel equilibrium swelling time, so we ignore the change in water content of SMH. To reduce experimental chance errors, each experiment was repeated three times. Figure 4 shows the tensile specimen and the result of isothermal uniaxial tensile tests. The stretch curve of SMH is similar to that of rubber and the initial modulus of SMH gradually increases with increasing temperature which may be related to the conformational transition of the PNIPAM chain.

The equilibrium mass water content  $\phi_w$  of SMH at different temperatures has been tested in [7] and we assume that the relationship between  $\phi_w$  and temperature is

$$100\phi_w = a \ln(|T - 300| + 1) \operatorname{Sgn}(T - 300) + b, \quad (19)$$

where  $a$  and  $b$  are the fitting parameters.  $\operatorname{Sgn}(x)$  is the signum function and it is defined as

$$\operatorname{Sgn}(x) = \begin{cases} 1 & x > 0 \\ 0 & x = 0 \\ -1 & x < 0. \end{cases} \quad (20)$$

In present constitutive model, the relationship between the volume fraction of the polymer network  $\phi$  and temperature is needed.  $\phi$  can be derived by  $\phi_w$  as

$$\phi = \frac{1 - \phi_w}{1 - (\alpha - 1)\phi_w}, \quad (21)$$

where  $\alpha$  is the density fraction of water to dry polymer. For most polymers,  $\alpha$  is close to 1, so here we take  $\alpha = 1$ . Then equation (21) can be simplified as

$$\phi = 1 - \alpha_w. \quad (22)$$

Through curve fitting, fitting parameters  $a$  and  $b$  were obtained. Figure 5(a) shows the result of curve fitting. We also fitted the low temperature ( $15^\circ\text{C}$ ) uniaxial stretching curve and the high temperature ( $45^\circ\text{C}$ ) stretching curve to obtain the parameters  $\mu_A$ ,  $n_A$ ,  $\mu_B$ ,  $n_B$ . As the polymer network is approximately incompressible, the bulk modulus and at low ( $15^\circ\text{C}$ ) and high ( $45^\circ\text{C}$ ) temperatures is approximated as  $K_A = 90\mu_A$  and  $K_B = 90\mu_B$ , respectively. The elastic modulus at other intermediate temperatures is determined by fitting uniaxial tensile stress–strain curves. According to equation (7), the elastic modulus of SMH is

$$E = 3f_C\mu_A + 3f_G\mu_B. \quad (23)$$

By fitting the experimental results, we obtained the parameters in equation (10). The fitting result is shown in figure 5(b) and the parameters of this constitutive model are summarized in table 1.

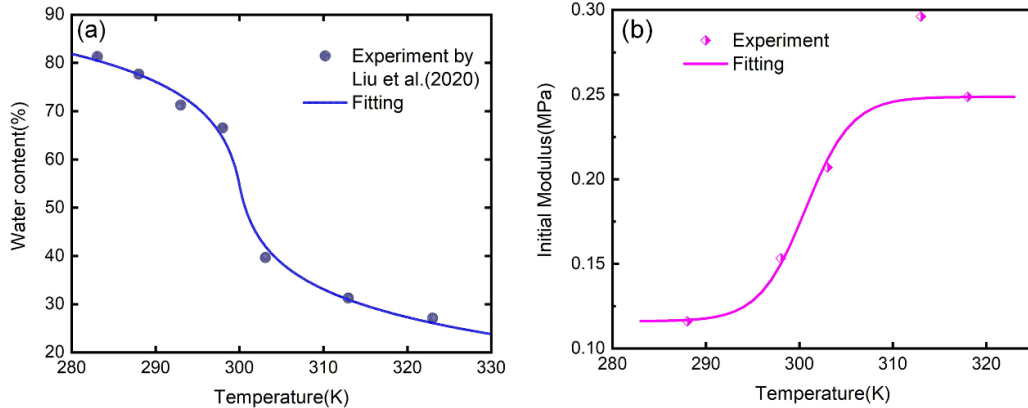


**Figure 5.** The fitting results: (a) the water content of SMH at different temperatures and (b) initial modulus of SMH at different temperatures.

**Table 1.** Material parameters of this model.

Notation	Variable	Value	Unit
$\mu_A$	Shear modulus of network A	0.0387	MPa
$\sqrt{n_A}$	Kuhn segment of network A	1.77	—
$\mu_B$	Shear modulus of network B	0.0829	MPa
$\sqrt{n_B}$	Kuhn segment of network B	2.76	—
$T_\theta$	Fitting constant of initial modulus	300.65	K
$\Delta$	Fitting constant of initial modulus	4.933	K
$a$	Fitting constant of water content	-8.966	—
$b$	Fitting constant of water content	54.604	—
$C_{10}$	Shear modulus of elastomer	2	MPa
$\gamma$	The ratio of current distance to maximum time of conformation transition of PNIPAM chain	0, 0.2, 0.4, 0.6, 0.8	—
$\Xi$	The ratio of experimental time to characteristic time of conformation transition of PNIPAM chain	0.5, 1, 5, 10, 100, $\infty$	—
$T_L$	Low temperature of shape memory cycle	288	K
$T_H$	High temperature of shape memory cycle	318	K
$\alpha$	Cooling related parameter	3, 4, 5	—
$\beta$	Heating related parameter	1, 1.5, 2	—
$A$	Parameter related with attenuation rate of the reference configuration of network B	0.5, 1	—
$\tau$	The time of the disappearance of shapememory effect in simulation	15	s

### 3.2. FE implementation

This section presents UMAT formulation based on the constitutive model in section 2. It is well known that the UMAT subroutine requires the material Jacobian matrix of the constitutive model. To avoid the tedious derivation of the material Jacobian matrix, we use a numerical method developed by [39, 46]. The form of material Jacobian matrix is

$$\mathcal{C} = \frac{1}{2J\varepsilon} (\tau(\mathbf{F}_+^{(ij)}) - \tau(\mathbf{F}_-^{(ij)})), \quad (24)$$

where  $\tau = J\sigma$  is Kirchhoff stress. It should be noted that we need to transform  $\tau$  into a corresponding  $1 \times 6$  row vector, and  $\mathcal{C}$  is a  $6 \times 6$  matrix in equation (24). Due to the symmetry of the  $\mathcal{C}$  matrix, the value of  $ij$  is further limited to  $ij = 11, 22, 33, 12, 13, 23$ . The deformation gradient increments are defined separately as

$$\begin{aligned} \mathbf{F}_+^{(ij)} &= \mathbf{F} + \Delta\mathbf{F}^{(ij)} \\ \mathbf{F}_-^{(ij)} &= \mathbf{F} - \Delta\mathbf{F}^{(ij)} \\ \Delta\mathbf{F}^{(ij)} &= \frac{\varepsilon}{2} (e_i \otimes e_j \mathbf{F} + e_j \otimes e_i \mathbf{F}), \end{aligned} \quad (25)$$

where  $\varepsilon$  is the perturbation coefficient and we take  $\varepsilon = 10^{-8}$ . More details about the material Jacobian matrix can be found in [39, 46].

## 4. Results and discussions

With the UMAT subroutine, we implemented the constitutive model into ABAQUS software. Notice that the characteristic time of conformation transition time (less than 10 ms [47]) is much less than the experimental time (min) and the programming deformation is not very large during shape memory

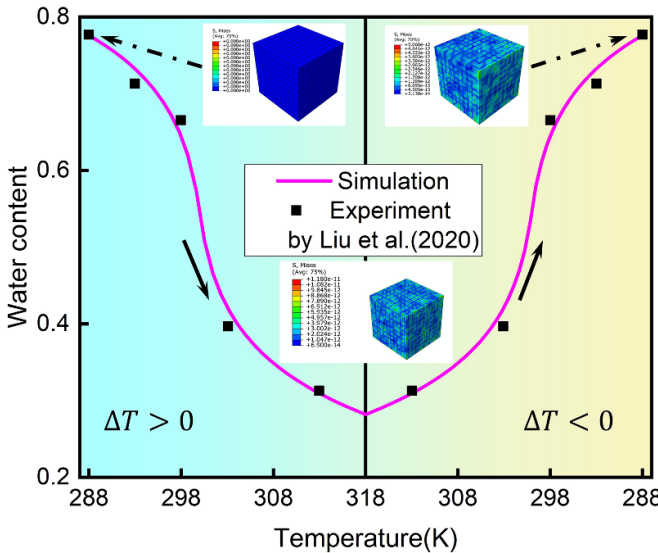


**Figure 6.** Numerical simulations and experimental results of the water content of the SMH at different temperatures.

cycles. Therefore, disregarding to the effect of  $\Xi$  and  $\gamma$  on fraction of globule chain, we simulated equilibrium swelling, isothermal uniaxial tension, reversible shape memory behavior and multiple shape memory cycles of SMHs and compared the simulation results and the experimental results. Then the effect of  $\Xi$  and  $\gamma$  on the shape memory effect is discussed later. All results are presented in the following.

#### 4.1. Equilibrium swelling

We established a cube and simulated the equilibrium swelling process of SMHs. A 20-node quadratic brick and hybrid with reduced integration elements (C3D20RH) were used in this simulation and the size of element was  $1\text{ mm} \times 1\text{ mm} \times 1\text{ mm}$ . The temperature change during the analysis was  $288\text{ K} \rightarrow 318\text{ K} \rightarrow 288\text{ K}$ . Figure 6 shows the comparison between simulation results with experimental results obtained by [7]. Since we divide the overall deformation into equilibrium swelling deformation and elastic deformation in the present constitutive model, there is also equilibrium swelling deformation so the SMH is in stress free state. In addition, the regularity between temperature and water content satisfies the same law during the warming or cooling process. This example initially verifies the effectiveness of UMAT subroutine.

#### 4.2. Isothermal uniaxial tension simulation

We set up three-dimensional geometric models with the same boundary conditions as the isothermal temperature uniaxial tension experiments. A 20-node quadratic brick and hybrid (C3D20H) were used in this simulation. Note that our model is based on hyperelastic model, so the time of the analysis step has no effect on the simulation results. Comparisons of the simulated and experimental results for isothermal uniaxial tension are shown in figure 7. Obviously, this model

can capture the isothermal mechanical properties of SMH at different temperatures.

#### 4.3. Reversible shape memory behavior

By simulating shape memory process, we validated the capability of this model to forecast the mechanical behavior of SMHs. Reversible shape memory cycle experiments in bending deformation mode were carried out in [7]. Rectangular specimens with the size of  $12\text{ mm} \times 3\text{ mm} \times 0.5\text{ mm}$  are folded in the middle along their length and the temperature-controlled shape memory behavior of SMH is described by the bending angle. We note that there is little change in angle along the width direction during this process. For this reason, we simplify the process to a plane strain problem. We set up two-dimensional geometric models with the size of  $12\text{ mm} \times 0.5\text{ mm}$  as shown in figure 8 and all element type are eight-node biquadratic plane strain with reduced integration and hybrid (CPE8RH). We divide the entire model equally into three segments. The left boundary of the middle segment is fixed, the right boundary is coupled to a reference point and the programmed deformation is a  $180^\circ$  rotation of this reference point.

In the experiment of Liu *et al* [7], shape fixed and shape recovery processes are carried out at constant low  $T_L$  or high  $T_H$  temperature. During this process, heat conduction and a non-equilibrium conformational transition of the PNIPAM molecular chain take place which take a long time to reach equilibrium. We consider this process to a temperature-controlled equilibrium problem by introducing a normalized time  $\omega = t'/t_{eq}$  ( $0 \leq \omega \leq 1$ ), where  $t'$  is actual time and  $t_{eq}$  represents the time to change temperature. The result of this treatment is that we cannot set a uniformly varying temperature during simulations because the reaction rate is faster at first, and then gradually slows down according to chemical knowledge. For this reason, we set the relationship between temperature and normalized time when simulating as

$$T = \begin{cases} T_L + (T_H - T_L)\exp\left(\frac{\alpha\omega}{\omega-1}\right) & \Delta T < 0 \\ T_H - (T_H - T_L)\exp\left(\frac{\beta\omega}{\omega-1}\right) & \Delta T > 0 \end{cases}, \quad (26)$$

where  $\alpha, \beta$  are two parameters and the comparisons of simulation and experimental results are shown in figures 9(a) and (b). These show that simulation results best match experimental results when  $\alpha = 5, \beta = 2$ . So we use this set of values in the later simulations.

#### 4.4. Multiple shape memory cycles

In addition to single reversible shape memory cycle, multiple shape memory cycles of the SMHs is also studied. The FE model in section 4.3 is used here and we simulate five shape memory cycles. The change in angle during the shape memory cycle is controlled by the parameter  $A$  and a comparison of the simulation results for different  $A$  with the experimental results is shown in figure 10(a). Shape fixity ratio described

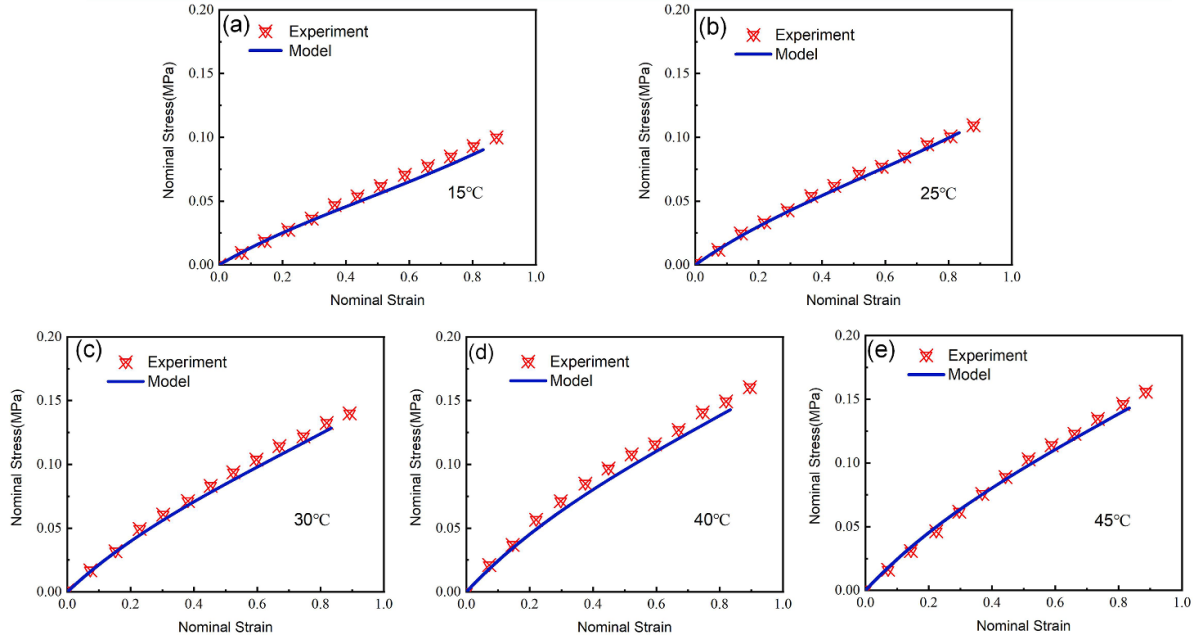


**Figure 7.** The results of numerical simulations and experiments of the SMH from isothermal temperature uniaxial tension.

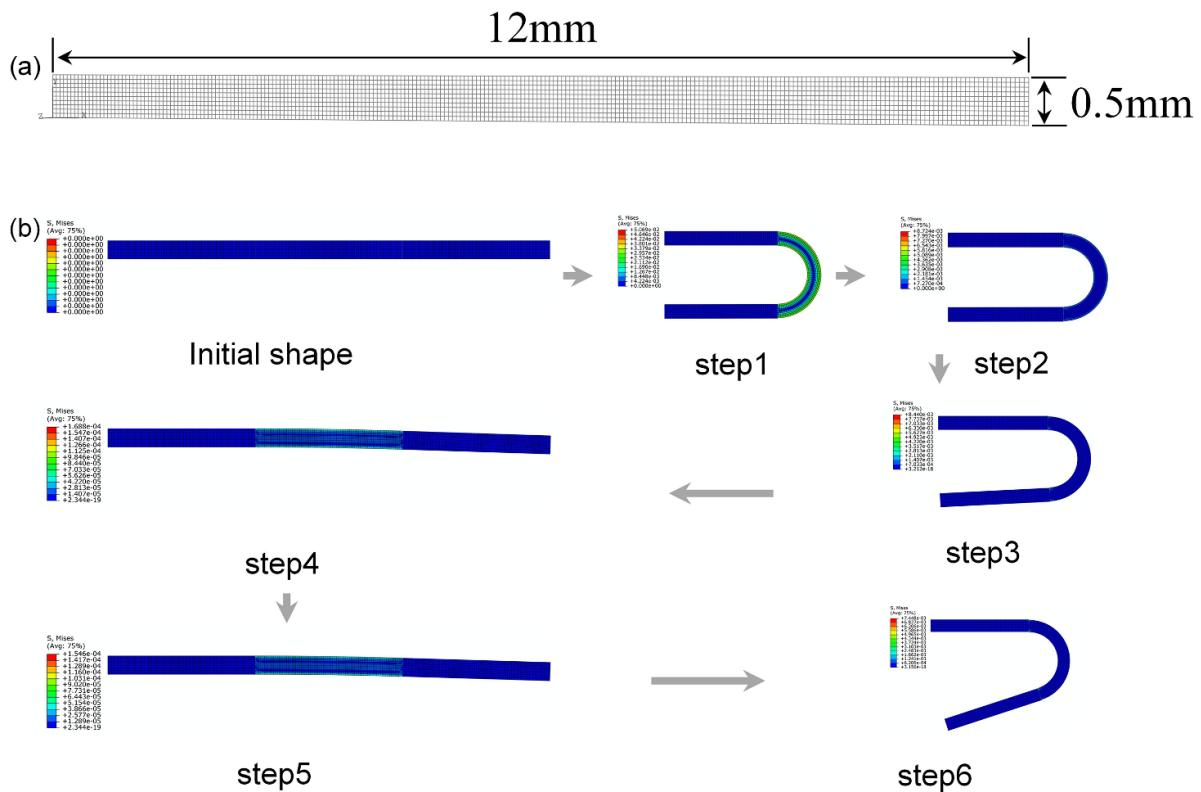


**Figure 8.** (a) Mesh of the finite element model. (b) Snapshots of the SMH during single reversible shape memory cycle, step 1: deformed at low temperature ( $15^{\circ}\text{C}$ ), step 2: maintaining its deformed shape and increasing temperature to  $45^{\circ}\text{C}$ , step 3: unloading at high temperature ( $45^{\circ}\text{C}$ ), step 4: decreasing temperature to  $15^{\circ}\text{C}$ , step 5: the purpose of this step is to accumulate the low temperature immersing time, step 6: reheating temperature to  $45^{\circ}\text{C}$ .

by rotation angle at high temperature decreases while shape recovery ratio described by rotation angle at low temperature is almost unchanged during multiple shape memory cycles,

which is basically in agreement with the experimental observation [7]. Figure 10(b) is the curve between rotation angle and temperature, which shows that SMH has different paths from

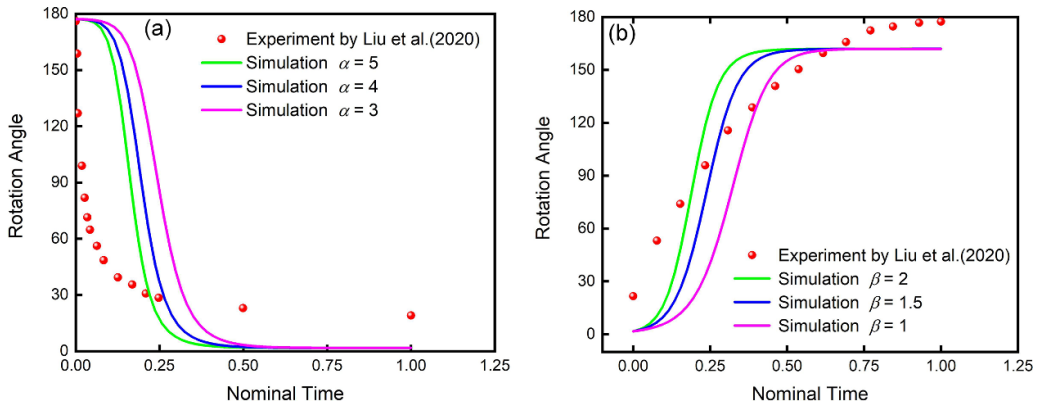


**Figure 9.** Experimental results and numerical simulations of rotation angle of SMH from single reversible shape memory cycle: (a) at different  $\alpha$  value and (b) at different  $\beta$  value.

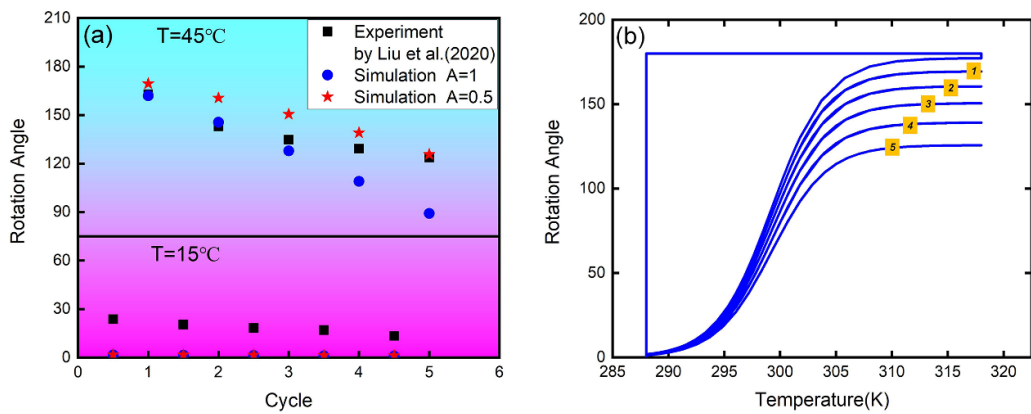


**Figure 10.** (a) The comparisons of simulation results with experimental results of rotation angle during multiple shape memory cycles. (b) The simulation result of rotation angle and temperatures during multiple shape memory cycles.

low to high temperature, while paths are not updated from high to low temperature due to the parameter  $\varpi$  in equation (18) is changes only when SMH is immersed in low temperature water.

In addition, this model can also be used to simulate more complex and useful deformation behaviors of SMHs. As a typical example, figures 11(a) and (b) show the FE model and the simulation results of the simplified model of soft robot grippers or drug release structures, respectively. The reversible shape memory effect of the SMH allows it to transform between shape A and shape B to accomplish grasping or drug release. This model can be used as an effective simulation tool for mechanical design in the fields of drug release, soft robotics and so on.

#### 4.5. Discussion

In above simulations, we validate the constitutive model of SMHs with simple examples. In this section, we further investigate the effects of time ratio and amount of deformation on shape fixity ratio ( $R_f$ ) and shape recovery ratio ( $R_c$ ).

We investigate the effect of  $\Xi$  and  $\gamma$  on the shape memory process using a classic example on surface instability of

hydrogel [48, 49]. As shown in figure 12, the plane strain finite element model is composed of a layer of SMH with small modulus and a thin layer of an elastomer with big modulus bonded to SMH. The constitutive model this elastomer is incompressible neo-Hooke model and the form of free energy is

$$W = C_{10}(I_1 - 3), \quad (27)$$

where,  $C_{10}$  is the shear modulus and here we let  $C_{10} = 2 \text{ MPa}$ . The boundary conditions are given as follows

$$\begin{cases} u_x = 0, u_y = 0, R_{xy} = 0, & \text{at the left} \\ u_y = 0, R_{xy} = 0, & \text{at the right and bottom.} \end{cases} \quad (28)$$

Four steps are created and the programming deformation is a compression of 10 mm at the right boundary. CPE8RH element is used for both elastomer and SMH. Figure 13 shows snapshot of SMH-elastomer system after deformed. Unlike previous studies, the surface instability is produced by compressive deformation and fixed by the temporary shape of the SMHs. Surface instability disappears as the SMH returns to its initial shape.

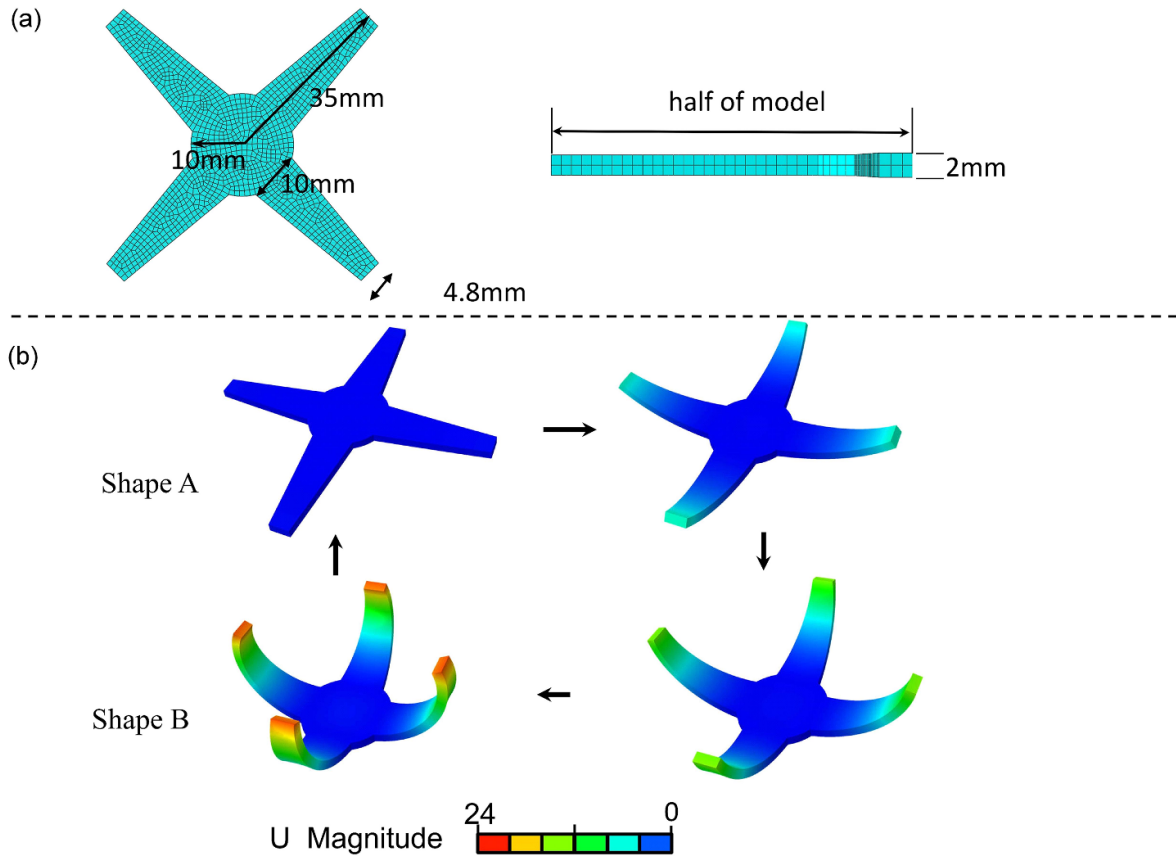


**Figure 11.** (a) Size and mesh of the simplified model of soft robot grippers or drug release structures. (b) The simulation results of this 3D structure during reversible shape memory cycle.

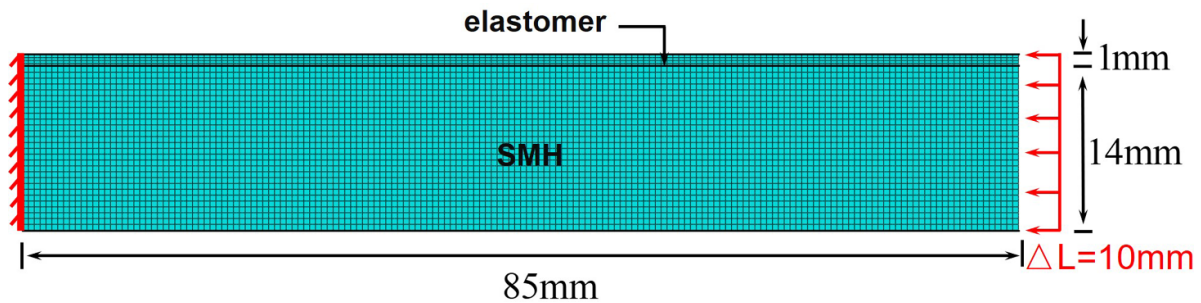


**Figure 12.** Geometry, mesh and boundary conditions of plane-strain finite element model.

$R_f$  and  $R_c$  are defined as

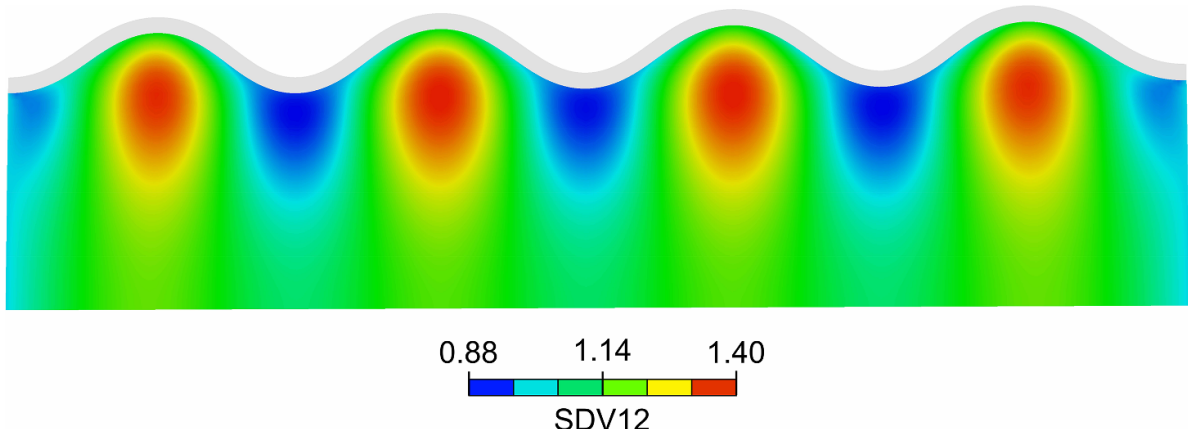
$$R_f = \frac{L_f}{L} \times 100\% \quad (29)$$

$$R_c = \frac{L_f - L_c}{L_f} \times 100\%$$

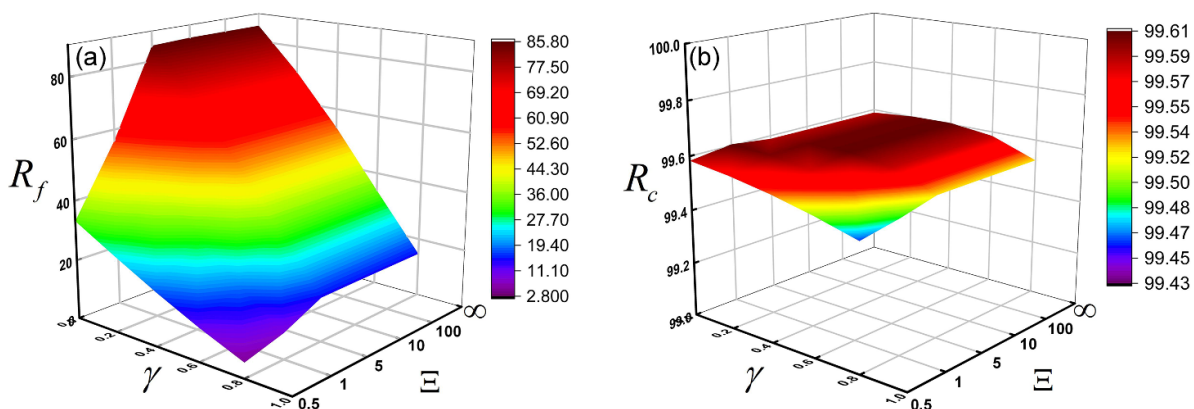
respectively, where  $L$  is programming deformation,  $L_f$  is the distance between right condition after unloading and right condition in initial condition and  $L_c$  is the between right condition after cooling and right condition in initial condition.

Figure 14 show the results of  $R_f$  and  $R_c$  in  $\gamma = 0, 0.2, 0.4, 0.6, 0.8$  and  $\Xi = 0.5, 1, 5, 10, 100, \infty$ . Obviously,

$\Xi$  has greater effect on shape fixity ratio and  $R_f$  gradually decreases as  $\Xi$  decreasing, especially when experimental time close to or less than the characteristic time of conformational transition (figure 14(a)). This result means that the experimental time needs to be much larger than the conformational transition time in order to have a high shape fixity rate.  $R_f$  decreases as  $\gamma$  increasing, but high shape fixity rate is achieved as  $\gamma$  is not close to 1 to.  $\Xi$  and  $\gamma$  have little effect on the shape recovery rate (figure 14(b)). However, this model does not consider the coupling relationship between water diffusion and polymer network deformation. The coupling of deformation and water transport during shape memory cycle will be investigated later.



**Figure 13.** Geometry of SMH-elastomer model after programming deformation.



**Figure 14.** Plot of relationship between  $\Xi$ ,  $\gamma$  and the property of SMH from numerical simulations of shape memory process: (a) shape fixity ratio, (b) shape recovery ratio.

## 5. Conclusion

A three-dimensional constitutive model and its numerical implementation of two-way SMHs are studied. The shape memory mechanism is that coil PNIPAM is transformed into globule state due to hydrophobic interaction after temperature increases, which fixes the temporary shape and vice versa. This inspires us to divide the SMH network into two parts composed of coil and globule PNIPAM, respectively and the fraction of which are mainly controlled by temperature. By changing reference configuration of globule PNIPAM network and considering its evolution equation, the reversible shape memory behavior of SMH and its attenuation during multiple shape memory cycles are considered. This model is implemented into a UMAT using a kind of a numerical method with wide applicability. We simulate the equilibrium swelling, isothermal uniaxial tension, reversible shape memory behavior and multiple shape memory cycles of SMH and simulated results were consistent with the experimental observations.

We show that our model can well capture the variation of water content during equilibrium swelling and isothermal uniaxial tension behaviors of SMHs. This model can also predict reversible shape memory behavior of SMHs, which shows shape fixity ratio decreases and shape recovery ratio

is almost unchanged during multiple shape memory cycles, in agreement with experimental results. In addition, the effects of time ratio and amount of deformation on shape fixity ratio and shape recovery ratio are further discussed, which shows that shape fixity ratio decreases as time ratio decreasing and the stretching amount increasing while time ratio and stretching amount have little effect on the shape recovery rate. For other SMH material systems, the constitutive model also is applied applicable by changing the corresponding physical parameters with physical significance. This work can provide guidance on the application of SMHs in fields of biomedical and soft robotics.

## Data availability statement

The data that support the findings of this study are available upon reasonable request from the authors.

## Acknowledgments

This work is supported by the National Natural Science Foundation of China (Grant No. 12072094) and the Heilongjiang Touyan Innovation Team Program.

## Appendix. Detailed derivation of constitutive model

The velocity gradient  $\mathbf{L}$  is defined as the derivative of velocity to Eulerian coordinates

$$\mathbf{L} = \frac{\partial \mathbf{v}}{\partial \mathbf{x}} = \dot{\mathbf{F}}\mathbf{F}^{-1}. \quad (\text{A.1})$$

Substituting equation (1) into equation (A.1) and considering  $\mathbf{F}_S$  is a diagonal matrix. We derive the velocity gradient of swelling part, the two parts of network as

$$\begin{aligned} \mathbf{L}_S &= \mathbf{D}_S = \frac{1}{3}(\mathbf{j}_S \mathbf{J}_S^{-1})\mathbf{I}, \\ \mathbf{L}_A &= \mathbf{L}_M, \\ \mathbf{L}_B &= \mathbf{L}_M - \mathbf{F}_B \bar{\mathbf{L}}(\mathbf{F}_B)^{-1}, \end{aligned} \quad (\text{A.2})$$

respectively, where  $\bar{\mathbf{L}} = \dot{\mathbf{H}}\mathbf{H}^{-1}$ . Then  $\mathbf{P} : \dot{\mathbf{F}}$  can be further written as

$$\begin{aligned} \mathbf{P} : \dot{\mathbf{F}} &= \frac{1}{2}\mathbf{T}_M : \dot{\mathbf{C}}_M + \frac{1}{3}J_M \text{tr}(\boldsymbol{\sigma})\mathbf{j}^S \\ &= J_M \boldsymbol{\sigma}_M : \mathbf{D}_M + \frac{1}{3}J_M \text{tr}(\boldsymbol{\sigma})\mathbf{j}^S \\ &= J_A \boldsymbol{\sigma}_A : \mathbf{D}_A + J_B \boldsymbol{\sigma}_B : \mathbf{D}_B + \frac{1}{3}J_M \text{tr}(\boldsymbol{\sigma})\mathbf{j}^S \\ &= J_A \boldsymbol{\sigma}_A : \mathbf{D}_A + J_B \boldsymbol{\sigma}_B : \mathbf{D}_B + \frac{1}{3}J_M \text{tr}(\boldsymbol{\sigma})\mathbf{j}^S + \beta. \end{aligned} \quad (\text{A.3})$$

Using equation (A.3), equation (3) can be further written as

$$\begin{aligned} \dot{\psi} + \eta \dot{T} - J_A \boldsymbol{\sigma}_A : \mathbf{D}_A - J_B \boldsymbol{\sigma}_B : \mathbf{D}_B - \beta \\ + \bar{P} \mathbf{j}^S - \mu \dot{c} + \frac{1}{T} \mathbf{q}_R \cdot \nabla T + \mathbf{j}_R \cdot \nabla \mu \leqslant 0, \end{aligned} \quad (\text{A.4})$$

where

$$\bar{P} = -\frac{1}{3}J_M \text{tr}(\boldsymbol{\sigma}) \quad (\text{A.5})$$

and

$$\beta = \frac{J}{2} \boldsymbol{\sigma}_B : \left[ (\mathbf{F}_B \bar{\mathbf{L}} \mathbf{F}_B^{-1}) + (\mathbf{F}_B \bar{\mathbf{L}} \mathbf{F}_B^{-1})^T \right]. \quad (\text{A.6})$$

The derivative the Helmholtz free energy density function with respect to time is

$$\dot{\psi} = \frac{\partial \psi}{\partial \mathbf{C}_A} : \dot{\mathbf{C}}_A + \frac{\partial \psi}{\partial \mathbf{C}_B} : \dot{\mathbf{C}}_B + \frac{\partial \psi}{\partial c} \dot{c} + \frac{\partial \psi}{\partial T} \dot{T}. \quad (\text{A.7})$$

To establish the relationship between free energy and stress, the first two terms of the above equation are further written as [50]

$$\begin{aligned} \frac{\partial \psi}{\partial \mathbf{C}_X} : \dot{\mathbf{C}}_X &= \frac{\partial \psi}{\partial \mathbf{C}_X} : ((\dot{\mathbf{F}}_X)^T \mathbf{F}_X + (\mathbf{F}_X)^T \dot{\mathbf{F}}_X) \\ &= 2\mathbf{F}_X \frac{\partial \psi}{\partial \mathbf{C}_X} (\mathbf{F}_X)^T : \mathbf{D}_X. \quad (X = A, B) \end{aligned} \quad (\text{A.8})$$

By substituting equation (A.8) into equation (A.7) and then substituting them into equation (A.4), the thermodynamic inequality can finally be concluded as

$$\begin{aligned} &\left( 2\mathbf{F}_A \frac{\partial \psi}{\partial \mathbf{C}_A} (\mathbf{F}_A)^T - J_A \boldsymbol{\sigma}_A \right) : \mathbf{D}_A \\ &+ \left( 2\mathbf{F}_B \frac{\partial \psi}{\partial \mathbf{C}_B} (\mathbf{F}_B)^T - J_B \boldsymbol{\sigma}_B \right) : \mathbf{D}_B \\ &+ \left( \frac{\partial \psi}{\partial c} - \mu_{\text{act}} \right) \dot{c} + \left( \frac{\partial \psi}{\partial T} - \eta \right) \dot{T} - \beta \\ &+ \frac{1}{T} \mathbf{q} \cdot \nabla T + \mathbf{j} \cdot \nabla \mu \leqslant 0. \end{aligned} \quad (\text{A.9})$$

For arbitrary  $\mathbf{D}_A, \mathbf{D}_B, \dot{c}, \dot{T}, \nabla T, \nabla \mu$ , the above inequality is required to be satisfied.  
we obtain

$$\begin{aligned} \boldsymbol{\sigma} &= \boldsymbol{\sigma}_A + \boldsymbol{\sigma}_B = \frac{2}{J_A} f_C \mathbf{F}_A \frac{\partial \psi_A}{\partial \mathbf{C}_A} (\mathbf{F}_A)^T + \frac{2}{J_B} f_G \mathbf{F}_B \frac{\partial \psi_B}{\partial \mathbf{C}_B} (\mathbf{F}_B)^T \\ \mu_{\text{act}} &= \frac{\partial \psi}{\partial c} \\ \mu &= \mu_{\text{act}} + \bar{P} \nu \\ \eta &= -\frac{\partial \psi}{\partial T} \\ -\beta &+ \frac{1}{T} \mathbf{q} \cdot \nabla T + \mathbf{j} \cdot \nabla \mu \leqslant 0. \end{aligned} \quad (\text{A.10})$$

In above equations, the first equation represents the Cauchy stress of the SMH, which is obtained by adding the stress of networks A and B and the stress from the derivative of  $f_C, f_G$  with respect to  $\mathbf{C}$  are ignored. The second and third equations represent the chemical potential, the fourth equation is used to calculate entropy and the fifth equation represents the dissipation term.

## ORCID iDs

Yanju Liu  <https://orcid.org/0000-0001-8269-1594>  
Jinsong Leng  <https://orcid.org/0000-0001-5098-9871>

## References

- [1] Zhang Y, Gao H, Wang H, Xu Z, Chen X, Liu B, Shi Y, Lu Y, Wen L and Li Y 2018 *Adv. Funct. Mater.* **28** 1705962
- [2] Zhang Y, Liao J, Wang T, Sun W and Tong Z 2018 *Adv. Funct. Mater.* **28** 1707245
- [3] Lowenberg C, Julich-Gruner K K, Neffe A T, Behl M and Lendlein A 2020 *Biomacromolecules* **21** 2024–31
- [4] Zhao Z, Zhang K, Liu Y, Zhou J and Liu M 2017 *Adv. Mater.* **29** 1701695
- [5] Osada Y and Matsuda A 1995 *Nature* **376** 219
- [6] Hu X, Zhang D and Sheiko S S 2018 *Adv. Mater.* **30** 1707461
- [7] Liu K et al 2020 *Adv. Mater.* **32** 2001693
- [8] Techawanitchai P, Idota N, Uto K, Ebara M and Aoyagi T 2012 *Sci. Technol. Adv. Mater.* **13** 064202
- [9] Drury J L and Mooney D J 2003 *Biomaterials* **24** 4337–51
- [10] Shang J, Le X, Zhang J, Chen T and Theato P 2019 *Polym. Chem.* **10** 1036–55
- [11] Cai S and Suo Z 2011 *J. Mech. Phys. Solids* **59** 2259–78
- [12] Song K, Zhu W, Li X and Yu Z 2020 *Mater. Lett.* **260** 126884

- [13] Zhou S, Zhou Q, Wang M, Zhang Z and Ren L 2020 *Int. J. Food Prop.* **23** 470–80
- [14] Xue Y, Lei J and Liu Z 2022 *Polymer* **243** 124623
- [15] Toh W, Ng T Y, Hu J and Liu Z 2014 *Int. J. Solids Struct.* **51** 4440–51
- [16] Huang R, Zheng S, Liu Z and Ng T Y 2020 *Int. J. Appl. Mech.* **12** 2050014
- [17] Ge Q, Luo X, Rodriguez E D, Zhang X, Mather P T, Dunn M L and Qi H J 2012 *J. Mech. Phys. Solids* **60** 67–83
- [18] Gu J, Leng J and Sun H 2017 *Mech. Mater.* **111** 1–14
- [19] Su X and Peng X 2018 *Int. J. Plast.* **110** 166–82
- [20] Li Y, He Y and Liu Z 2017 *Int. J. Plast.* **91** 300–17
- [21] Yan C, Yang Q and Li G 2020 *Int. J. Mech. Sci.* **177** 105552
- [22] Lu W, Le X, Zhang J, Huang Y and Chen T 2017 *Chem. Soc. Rev.* **46** 1284–94
- [23] Perera M M and Ayres N 2020 *Polym. Chem.* **11** 1410–23
- [24] Zhang Y, Li Y and Liu W 2015 *Adv. Funct. Mater.* **25** 471–80
- [25] Drozdov A 2014 *Eur. Phys. J. E* **37** 1–13
- [26] Ptitsyn O, Kron A and Eizner Y Y 1967 *J. Polym. Sci. C* **16** 3509–17
- [27] Wu C and Wang X 1998 *Phys. Rev. Lett.* **80** 4092
- [28] Chen Y, Zhang H, Chen J, Kang G and Hu Y 2021 *Acta Mech. Sin.* **37** 748–56
- [29] Govindjee S and Simo J 1991 *J. Mech. Phys. Solids* **39** 87–112
- [30] Machado G, Chagnon G and Favier D 2014 *J. Mech. Phys. Solids* **63** 29–39
- [31] Lee E H 1969 *J. Appl. Mech.* **36** 1–6
- [32] Zhao Z, Wu D, Lei M, Zhang Q, Wang P and Lei H 2021 *Int. J. Solids Struct.* **229** 111135
- [33] Das S and Roy D 2021 *Int. J. Mech. Sci.* **196** 106290
- [34] Chester S A and Anand L 2011 *J. Mech. Phys. Solids* **59** 1978–2006
- [35] Mao Y, Chen F, Hou S, Qi H J and Yu K 2019 *J. Mech. Phys. Solids* **127** 239–65
- [36] Flory P J 1942 *J. Chem. Phys.* **10** 51–61
- [37] Huggins M L 1942 *J. Phys. Chem.* **46** 151–8
- [38] Arruda E M and Boyce M C 1993 *J. Mech. Phys. Solids* **41** 389–412
- [39] Johnsen J, Clausen A H, Grytten F, Benallal A and Hopperstad O S 2019 *J. Mech. Phys. Solids* **124** 681–701
- [40] Halperin A and Goldbart P M 2000 *Phys. Rev. E* **61** 565
- [41] Zhu P W and Napper D H 1997 *J. Chem. Phys.* **106** 6492–8
- [42] Wang X, Qiu A X and Wu C 1998 *Macromolecules* **31** 2972–6
- [43] Graziano G 2000 *Int. J. Biol. Macromolecules* **27** 89–97
- [44] Park H, Harrison P, Guo Z, Lee M G and Yu W R 2016 *Mech. Mater.* **93** 43–62
- [45] Qi H J, Nguyen T D, Castro F, Yakacki C M and Shandas R 2008 *J. Mech. Phys. Solids* **56** 1730–51
- [46] Miehe C 1996 *Comput. Methods Appl. Mech. Eng.* **134** 223–40
- [47] Wang X Y, Fana H Y, Yea X D, Liua B and Lin S 2018 *Chin. J. Chem. Phys.* **31** 789
- [48] Bouklas N, Landis C M and Rui H 2015 *J. Mech. Phys. Solids* **79** 21–43
- [49] Tanaka T, Sun S T, Hirokawa Y, Katayama S, Kucera J, Hirose Y and Amiya T 1987 *Nature* **325** 796–8
- [50] Shen F, Kang G, Lam Y C, Liu Y and Zhou K 2019 *Int. J. Plast.* **121** 227–43